# Title: Biofilm self-patterning: mechanical force landscaping drives a collective reorientation cascade

**Authors:** Japinder Nijjer[1], Changhao Li[2], Qiuting Zhang[1], Haoran Lu[1], Sulin Zhang[2,3*], Jing Yan[1,4*]

**Affiliations:**

[1]Department of Molecular, Cellular and Developmental Biology, Yale University, New Haven, CT, USA.

[2]Department of Engineering Science and Mechanics, Pennsylvania State University, University Park, PA, USA.

[3]Department of Biomedical Engineering, Pennsylvania State University, University Park, PA, USA.

[4]Quantitative Biology Institute, Yale University, New Haven, CT, USA.

*Corresponding author. Email: suz10@psu.edu or jing.yan@yale.edu

**Abstract:** During development, cells often self-organize into distinctive patterns with long-range orientational order. However, the mechanism by which long-range order emerges through complex interactions, particularly in the prokaryotic domain, remains elusive. Here we report, in growing *Vibrio cholerae* biofilms, a reorientation cascade consisting of cell verticalization in the core and radial alignment in the rim, generating a pattern reminiscent of a blooming aster. Single-cell imaging combined with agent-based simulations reveal that cell verticalization and radial alignment are spatiotemporally coupled, each generating the driving force for the other, to cause a dynamic cascade of differential orientational ordering. Such self-patterning is absent in nonadherent mutants but can be restored through opto-manipulation of growth. A two-phase active

nematic model is developed to elucidate the mechanism underlying biofilm self-patterning, which offers insights into the control of organization in complex bacterial communities.

**One-Sentence Summary:** Bacterial biofilms robustly pattern themselves through orientation-dependent, growth induced flows.

**Main Text:**

The spatiotemporal patterning of cells is a fundamental morphogenetic process that has profound effects on the phenotypes and functions of multicellular organisms (*1–3*). In the prokaryotic domain, bacteria are often observed to form organized multicellular communities known as biofilms, which are detrimental due to persistent infections, clogging of flows, and surface fouling (*4*, *5*), but can be beneficial in the context of wastewater treatment (*6*) and microbial fuel cells (*7*). During development, biofilms exhibit macroscopic morphological features ranging from wrinkles, blisters, to folds (*8–10*). At the cellular scale, recent progress in single-cell imaging has revealed the reproducible three-dimensional architecture of biofilms (*11–13*). However, how the cellular ordering emerges from individual bacterium trajectories remains poorly understood. In particular, it remains unclear how cell proliferation is coordinated with intercellular interactions in a growing biofilm to elicit robust self-patterning against bacteria's inherent tendency to grow in an unstructured manner (*14–16*). An understanding of how individual cell growth links to collective patterning as a result of self-generated forces can provide insights into the mechanobiology of bacterial biofilms, their responses to environmental and biotic stresses (*17*), and the engineering of nonliving active-matter analogs (*18*, *19*).

To bridge the gap between interactions at the cellular scale and patterns at the community scale, here we combine single-cell imaging and agent-based simulations to reveal the underlying

mechanism for self-patterning in biofilm formed by *Vibrio cholerae*, the causal agent of the pandemic cholera. We observe that biofilm-dwelling bacteria self-organize into an aster pattern, which emerges from a robust reorientation cascade, involving cell verticalization in the core and radial alignment in the growing rim. We reveal that the verticalized core generates directional flow that drives radial alignment of the cells in the periphery, while the radially aligned rim generates compressive stresses that expand the verticalized core, leading to a robust, inter-dependent differential orientational ordering. Based on these findings, we derive a two-phase active nematic model for biofilm self-patterning, which is potentially generalizable to other developmental systems with growth-induced flows (*20*, *21*). Our findings suggest that the self-generated cellular force landscape, rather than chemical signaling or morphogen gradients as often seen in eukaryotic cells (*22*), controls pattern formation in biofilms.

## *V. cholerae* biofilms self-organize into aster patterns

We imaged the growth of *V. cholerae* biofilms confined between glass and an agarose gel at single-cell resolution (Fig. 1A). We used a constitutive biofilm producer locked in a high c-di-GMP state (*23*) and focused on the biophysical aspects of self-organization. To further simplify our studies, we focused on a mutant missing the cell-to-cell adhesion protein RbmA – this strain is denoted as WT* – although our analysis also applies to strains with cell-to-cell adhesion (fig. S1). Using confocal microscopy, the 3D architecture of the biofilms was captured over time from single founder cells to mature biofilms consisting of thousands of cells (Fig. 1B and movie S1). An adaptive thresholding algorithm was used to segment individual cells in the confined 3D biofilm (fig. S2, Supplementary Text) from which the location and direction of each rod-shaped bacterium were identified (Fig. 1, C to F). Strikingly, cells in the basal layer *reproducibly* self-organized into

an aster pattern, consisting of a core with tilted or "verticalized" cells and an outward splaying rim with radially aligned cells (Fig. 1D and fig. S3).

We quantified the degree of cell ordering in the basal layer using a radial order parameter (*24*), $S = 2\langle(\hat{\boldsymbol{n}}_{\parallel} \cdot \hat{\boldsymbol{r}})^2\rangle - 1$, where $\hat{\boldsymbol{n}}_{\parallel}$ is the projection of the cell direction on the basal plane (Fig. 1G) and $\hat{\boldsymbol{r}}$ is the unit vector along the radial direction. $S$ equals 1 for cells that are aligned in an aster, $-1$ for cells that are aligned in a vortex, and 0 for cells that are randomly oriented. We found that cells in WT* biofilms exhibited a reproducible tendency to align radially ($S = 0.54 \pm 0.07$). Since previous work has shown that cell-to-surface adhesion controls colony biofilm morphology (*10*, *25*), we hypothesized that adhesion may play an important role in cell ordering as well. To test this hypothesis, we deleted the genes encoding cell-to-surface adhesion proteins Bap1 and RbmC (*26*–*28*) ($\Delta BC$) and found that the radial order was destroyed in the resulting biofilms: cells assumed random orientations in the basal plane with $S = 0.11 \pm 0.11$ (Fig. 1, E and G). Concomitant with the disorder was the absence of a verticalized core; most cells in the basal layer were parallel to the substrate. We further confirmed the importance of cell-to-surface adhesion by titrating *rbmC* expression: increasing cell-to-surface adhesion resulted in more verticalized cells and stronger radial alignment (Fig. 2H and fig. S4). Removing the extracellular matrix entirely by deleting the key *Vibrio* polysaccharide ($\Delta vpsL$) (*29*) resulted in locally aligned microdomains of horizontal cells without long-range order ($S = 0.02 \pm 0.08$, Fig 1, F and G), in line with previous studies on growing 2D bacterial colonies (*15*, *16*). These observations suggest that exopolysaccharide production controls a *local* order-to-disorder transition, whereas cell-to-surface adhesion controls a *global* order-to-disorder transition.

To determine whether a purely mechanical model could recapitulate the experimental observations, we extended previous agent-based simulations (ABSs) (*30*) that account for cell-to-cell and cell-to-surface interactions (Supplementary Text). Our ABSs reproduced the observed verticalized core and aster formation in adherent cells, and the absence of both in nonadherent cells, in agreement with experiments (fig. S5 and S6, and movie S2). This suggests that the emergent pattern originates primarily from mechanical interactions.

**Surface adhesion drives ordering through differential growth**

In molecular liquid crystals, a lower temperature favors order due to entropy; however, for out-of-equilibrium systems such as growing biofilms, the driving force for ordering is more complex. We hypothesized that radial organization arose from the coupling between the cells and their self-generated flow, inspired by the alignment of rod-shaped objects under fluid shear (*31*). Note that biofilm-dwelling cells are nonmotile, therefore, flow in this context is generated through cell growth and cell-cell interactions. To test our hypothesis, we tracked cell orientations and trajectories *simultaneously* during biofilm development by using strains expressing a single intracellular punctum (Fig. 2, A to E, fig. S7 and S8, and movie S3) (*32*). As WT* biofilms grew, cells towards the center tilted away from the substrate, developing a core of verticalized cells that expanded over time (Fig. 2C). The resulting growth-induced flow field had a zero-velocity core (Fig. 2D), corresponding to the verticalized cells that project their offspring into the third dimension (Fig. 1D). In contrast, in the nonadherent mutant, the velocity field simply scaled linearly with the radial position. From the measured velocity field, we extracted the *apparent* in-plane proliferation rate $g$ (Fig. 2B and 2D inset). We found that $g$ was uniform in the nonadherent biofilm: all cells in the basal layer were predominantly parallel to the substrate and therefore contributed to the basal layer expansion. In contrast, in the WT* biofilm, a growth void ($g \approx 0$)

emerged in the center, with nearly uniform growth in the outer growing rim. Concomitant with the initiation of differential growth, an aster pattern emerged, signified by a growing $S(r)$ with a rising peak (Fig. 2E).

**A reorientation cascade governs biofilm self-patterning**

The close connection between cell verticalization, growth-induced flow, and aster pattern formation inspired us to propose a reorientation cascade for biofilm self-patterning. First, cell-to-surface adhesion coupled with growth-induced mechanical stresses lead to *stably* anchored, verticalized cells in the biofilm center, which results in differentially oriented proliferation. Differential proliferation subsequently drives cellular flows that align the cells into an aster pattern, which further facilitates cell verticalization. Below, we theoretically analyze the inter-dependency of these two key steps.

**Step 1:** To illustrate the formation and stabilization of the verticalized core, we consider a reduced problem consisting of a spherocylindrical cell that is parallel and adhered to a substrate and squeezed by two neighbors (Supplementary Text). The resulting energy landscape displays two distinct mechanical instabilities (Fig. 2F). The first instability corresponds to the verticalization event reported earlier (*30*, *33*, *34*). Briefly, cells in a growing population mechanically push each other, generating pressure. This pressure accumulates and eventually exceeds a threshold, causing some cells to rotate away from the substrate (verticalize). The second instability corresponds to the "pinch-off" of these verticalized cells. In this case, neighboring cells generate forces in the out-of-plane direction that eject the verticalized cells from the substrate. For WT* cells, our analysis shows that pinching a vertical cell off the surface is energetically much more costly than verticalizing a horizontal cell. Therefore, pinch-off is kinetically hindered and verticalized cells

can *stably* inhabit the basal layer. The smaller the cell-to-surface adhesion, the smaller the energy difference between the two instabilities (fig. S9) and therefore, the less stable the verticalized cells. The energy difference vanishes in nonadherent cells, resulting in spontaneous ejection of mutant cells upon verticalization. This explains the absence of verticalized cells in the mutant biofilms and bacterial colonies (Fig. 1, E and F). In the WT* biofilm, verticalization preferentially occurs near the center where pressure is highest, leading to an expanding verticalized core (*30*). Since rod-shaped cells grow and divide along their long axis, this spatial segregation of cell orientation leads to spatially patterned differential growth.

**Step 2:** Next, we connect differential growth to self-patterning by applying active nematic theory (*19*, *35*). Consider first the response of a suspension of elongated particles to flow. Defining the nematic order parameter $\boldsymbol{Q} = 2\langle \hat{\boldsymbol{n}}_{\parallel} \otimes \hat{\boldsymbol{n}}_{\parallel} - \boldsymbol{I}/2 \rangle$ as the head-tail symmetric tensor representation of the cell orientation, mesoscopically averaged over a small region, its evolution in a surrounding flow $\boldsymbol{u}$ is given by (*36*)

$$(\partial_t + \boldsymbol{u} \cdot \nabla)\boldsymbol{Q} = \boldsymbol{S} + \Gamma \boldsymbol{H}, \tag{1}$$

where $\boldsymbol{S} = \lambda \boldsymbol{E} + \boldsymbol{\omega} \cdot \boldsymbol{Q} - \boldsymbol{Q} \cdot \boldsymbol{\omega}$ quantifies the driving force for the rod-shaped particles to rotate within a velocity gradient field. Here $\boldsymbol{E} = \frac{1}{2}[\nabla \boldsymbol{u} + \nabla \boldsymbol{u}^T - (\nabla \cdot \boldsymbol{u})\boldsymbol{I}]$ is the traceless strain-rate tensor, $\boldsymbol{\omega} = \frac{1}{2}(\nabla \boldsymbol{u} - \nabla \boldsymbol{u}^T)$ is the vorticity tensor, and $\lambda$ is the flow-alignment parameter. For rod-shaped objects, $\lambda > 0$, corresponding to a tendency for rods to align with flow streamlines (*14*). Finally, the nematic alignment term $\Gamma \boldsymbol{H}$ relaxes $\boldsymbol{Q}$ towards a bulk state with minimal angular variation. The $\Gamma \boldsymbol{H}$ term plays an important role in many passive and active nematic systems when the interparticle distance is small and the tendency to locally align is strong (*14–16*). However, its contribution in biofilms is expected to be negligible since cells are buffered from each other by

soft exopolysaccharides (See Supplementary Text). Assuming axisymmetry, the evolution of the cell orientation field is given by

$$\partial_t \Theta + u_r \partial_r \Theta = -f(r,t)\sin(2\Theta), \quad (2)$$

where $\Theta$ is the angle between the local orientation field and the radial direction, $f = (\lambda r/4q)\partial_r(u_r/r)$ quantifies the aligning torque due to gradients in the flow field, and $q$ quantifies the degree of local ordering (Supplementary Text). From $\partial_t \Theta \sim -f\sin(2\Theta)$, we find that a nonzero $f$ causes cells to rotate, and the direction of rotation is critically dependent on the sign of $f$.

Unlike passive liquid crystals, biofilm-dwelling cells generate their own velocity field through growth. Assuming uniform density, mass conservation requires $\nabla \cdot \boldsymbol{u} = g(r)$. In nonadherent mutant biofilms and bacterial colonies, growth is exclusively in-plane with a uniform growth rate $\gamma$, resulting in a linear velocity field, $u_r = \gamma r/2$, and thus a vanishing driving force for cell alignment ($f = 0$). Under this condition, cells are simply advected outwards without any tendency to align, leading to a disordered pattern. In contrast, in WT* biofilms, verticalization stabilizes an expanding in-plane growth void, $r_0(t)$. This corresponds to a differential growth rate $g(r)$: 0 for $r \leq r_0$ and $\gamma$ for $r > r_0$. The resulting velocity field is $\gamma(r - r_0^2/r)/2$ for $r > r_0$, leading to a *strictly positive* driving force for radial alignment, $f = \frac{\lambda\gamma r_0^2}{4qr^2} > 0$, in the outer growing rim. In this case, $\Theta$ dynamically approaches 0, characteristic of an aster (fig. S10). Our continuum theory thus reveals that differential growth, established by a verticalized core ($r_0 \neq 0$), generates the driving force for radial alignment in a growing biofilm. This driving force vanishes in the absence of a core ($r_0 = 0$), leading to a disordered phenotype.

**Imposing a growth void reproduces radial ordering**

A key prediction of the continuum theory is that a growth void is *sufficient* to induce radial organization. To test this prediction, we patterned a growth void into an otherwise disordered biofilm. Specifically, we started with a nonadherent biofilm that had been grown for 17 hours and used a 405 nm laser to selectively kill the cells in the center. The vestiges of the dead cells sustained a growth void (fig. S11), mimicking the verticalized core in the WT* biofilm. Consistent with our model prediction, the proliferating cells aligned radially over time in biofilms with a growth void, whereas biofilms without a growth void remained disordered (Fig. 3, A to C). Conversely, our theory predicts that *excess* growth at the biofilm center should lead to $f < 0$ and therefore to vortex formation (Supplementary Text). Indeed, in another set of experiments, we observed that the nonadherent cells aligned circumferentially when excess growth was introduced at the center (fig. S12). We also quantitatively tested the validity of the model by prescribing a growth void with a fixed size $r_0$ in a set of simplified 2D ABSs. We found that the instantaneous angular velocity of individual cells scaled linearly with $\sin(2\Theta)/r^2$ and that increasing $r_0$ led to a quadratic increase in the angular velocity, all in agreement with the theory (Fig. 3D and fig. S10 and 13). Note that in both simulations and experiments, the radial order quickly saturated in the patterned biofilm with a fixed $r_0$, because the aligning force decays with $1/r^2$ as cells are advected outward. Thus, a growing $r_0(t)$ is necessary to reinforce radial alignment during biofilm expansion. This is indeed the case in WT* biofilms: growth of the outer rim accumulates pressure to generate more verticalized cells, thereby expanding the verticalized core and continuously driving alignment in the outer horizontal cells. To interrogate the feedback between these two key reorientation steps, we next develop a minimal physical model coupling verticalization of individual cells to the long-range radial ordering.

**Two-phase model of cell organization**

We decompose the biofilm into populations of two phases with vertical and horizontal cells and take the phase fractions to be $\rho$ and $1-\rho$, respectively. The kinetic growths of the phases are governed by

$$\partial_t \rho + \nabla \cdot (\boldsymbol{u}\rho) = C(p)(1-\rho),$$

$$\partial_t (1-\rho) + \nabla \cdot \big(\boldsymbol{u}(1-\rho)\big) = \gamma(1-\rho) - C(p)(1-\rho). \quad \text{(3a,b)}$$

Here we assume that the horizontal-to-vertical transition is driven by the local pressure $p$, where $C(p)$ is a conversion rate. We further assume that pressure arises from friction $\nabla p = \eta \boldsymbol{u}$ where $\eta$ is the friction coefficient, and that only the horizontal cells generate growth in the basal layer, $\nabla \cdot \boldsymbol{u} = \gamma(1-\rho(\boldsymbol{r}))$. Together with Eq. (2), these equations generate a complete continuum description of the dynamics of cell growth and reorientation in biofilms (Supplementary Text). Numerical solutions of the model *quantitatively* reproduce the cascade of self-organization events (Fig. 4, A to D), showing the intimate spatiotemporal coupling between cell verticalization and radial alignment.

Many salient features of the experimental results are recapitulated by the model: for example, $S(r)$ reaches a maximum near the verticalized core where the driving force is the strongest. Interestingly, the model reveals a frozen core where cells cease to reorganize (compare Fig. 2E and Fig. 4D): as the in-plane velocity goes to zero, the driving force to rotate also vanishes – cells in the core are thus locked as a "fossil record" that memorizes the mechanical history they have experienced. Importantly, the model yields robust results: regardless of the initial conditions and choice of parameters (fig. S14), a WT* biofilm always patterns itself following the sequence

shown in Fig. 4E. Our two-phase active nematic model thus provides a reproducible mechanical blueprint that guides biofilm development.

## Discussion

Our results reveal a mechanically driven self-patterning mechanism in bacterial biofilms in which cells synergistically order into an aster pattern. Specifically, we showed that surface adhesion leads to stable cell verticalization, which in turn directs radial cell alignment during surface expansion. Evidently, this inter-dependent differential ordering involves biofilm-wide, bidirectional mechanical signal generation and transmission, in contrast to the biochemical signaling widely observed in other living organisms. In *On Growth and Form* (*37*), D'Arcy Thompson wrote: "… growth [is] so complex a phenomena…rates vary, proportions change, and the whole configuration alters accordingly." Although over a century old, this statement still rings true today. Our two-phase active nematic model provides a mathematical formalism for this statement in the context of bacterial biofilms.

Spontaneous flow generation is a common phenomenon in various developmental systems, including zebrafish embryonic development (*21*), ventral furrow formation in *Drosophila* (*20*), etc. While flow causes bulk morphological changes in these systems, in biofilms it acts to transmit mechanical forces and drive long-range internal organization. It is intriguing to contemplate whether the synchronous mechanical signaling between differentially grown cells and the resulting pattern could be generalized to other organisms with anisotropic growth of polarized cells. In a broader context, cell polarity and organization critically underlie collective cell function and normal development, as exemplified by topological defects that mediate 2D-to-3D transitions in motile bacterial colonies (*38*) and cell death and extrusion in epithelial layers (*39*). Our results here shed light on the biomechanical control of cell organization through the spatiotemporal patterning

of growth and pave the way to controlling cell organization by encoding synthetic biological circuits or optogenetic manipulation (*40*).

## References


1. T. Lecuit, L. Le Goff, Orchestrating size and shape during morphogenesis. *Nature* **450**, 189–192 (2007).

2. K. D. Irvine, B. I. Shraiman, Mechanical control of growth: ideas, facts and challenges. *Development* **144**, 4238–4248 (2017).

3. L. Hong, M. Dumond, M. Zhu, S. Tsugawa, C.-B. Li, A. Boudaoud, O. Hamant, A. H. K. Roeder, Heterogeneity and robustness in plant morphogenesis: from cells to organs. *Annu. Rev. Plant Biol.* **69**, 469–495 (2018).

4. L. Hall-Stoodley, J. W. Costerton, P. Stoodley, Bacterial biofilms: from the natural environment to infectious diseases. *Nat. Rev. Microbiol.* **2**, 95–108 (2004).

5. M. Ghannoum, M. Parsek, M. Whiteley, P. Mukherjee, *Microbial Biofilms* (ASM Press, Washington, DC, ed. 2, 2015).

6. S. Wuertz, P. Bishop, P. Wilderer, *Biofilms in wastewater treatment: an interdisciplinary approach* (IWA Publishing, London, UK, 2003).

7. A. E. Franks, N. Malvankar, K. P. Nevin, Bacterial biofilms: the powerhouse of a microbial fuel cell. *Biofuels* **1**, 589–604 (2010).

8. M. Asally, M. Kittisopikul, P. Rué, Y. Du, Z. Hu, T. Çağatay, A. B. Robinson, H. Lu, J. Garcia-Ojalvo, G. M. Süel, Localized cell death focuses mechanical forces during 3D patterning in a biofilm. *Proc. Natl. Acad. Sci. USA* **109**, 18891–18896 (2012).

9. M. Trejo, C. Douarche, V. Bailleux, C. Poulard, S. Mariot, C. Regeard, E. Raspaud, Elasticity and wrinkled morphology of *Bacillus subtilis* pellicles. *Proc. Natl. Acad. Sci. USA* **110**, 2011–2016 (2013).

10. J. Yan, C. Fei, S. Mao, A. Moreau, N. S. Wingreen, A. Košmrlj, H. A. Stone, B. L. Bassler, Mechanical instability and interfacial energy drive biofilm morphogenesis. *eLife* **8**, e43920 (2019).

11. K. Drescher, J. Dunkel, C. D. Nadell, S. van Teeffelen, I. Grnja, N. S. Wingreen, H. A. Stone, B. L. Bassler, Architectural transitions in *Vibrio cholerae* biofilms at single-cell resolution. *Proc. Natl. Acad. Sci. USA* **113**, E2066-2072 (2016).

12. J. Yan, A. G. Sharo, H. A. Stone, N. S. Wingreen, B. L. Bassler, *Vibrio cholerae* biofilm growth program and architecture revealed by single-cell live imaging. *Proc. Natl. Acad. Sci. USA* **113**, E5337–E5343 (2016).

13. R. Hartmann, P. K. Singh, P. Pearce, R. Mok, B. Song, F. Díaz-Pascual, J. Dunkel, K. Drescher, Emergence of three-dimensional order and structure in growing biofilms. *Nat. Phys.* **15**, 251–256 (2019).

14. A. Doostmohammadi, S. P. Thampi, J. M. Yeomans, Defect-mediated morphologies in growing cell colonies. *Phys. Rev. Lett.* **117**, 048102 (2016).

15. D. Dell'Arciprete, M. L. Blow, A. T. Brown, F. D. C. Farrell, J. S. Lintuvuori, A. F. McVey, D. Marenduzzo, W. C. K. Poon, A growing bacterial colony in two dimensions as an active nematic. *Nat. Commun.* **9**, 4190 (2018).

16. Z. You, D. J. G. Pearce, A. Sengupta, L. Giomi, Geometry and mechanics of microdomains in growing bacterial colonies. *Phys. Rev. X* **8**, 031065 (2018).

17. A. Dragoš, Á. T. Kovács, The peculiar functions of the bacterial extracellular matrix. *Trends Microbiol.* **25**, 257–266 (2017).

18. S. Ramaswamy, The mechanics and statistics of active matter. *Annu. Rev. Condens. Matter Phys.* **1**, 323–345 (2010).

19. M. C. Marchetti, J. F. Joanny, S. Ramaswamy, T. B. Liverpool, J. Prost, M. Rao, R. A. Simha, Hydrodynamics of soft active matter. *Rev. Mod. Phys.* **85**, 1143–1189 (2013).

20. B. He, K. Doubrovinski, O. Polyakov, E. Wieschaus, Apical constriction drives tissue-scale hydrodynamic flow to mediate cell elongation. *Nature* **508**, 392–396 (2014).

21. P. J. Keller, A. D. Schmidt, J. Wittbrodt, E. H. K. Stelzer, Reconstruction of zebrafish early embryonic development by scanned light sheet microscopy. *Science* **322**, 1065 (2008).

22. M. D. Petkova, G. Tkačik, W. Bialek, E. F. Wieschaus, T. Gregor, Optimal decoding of cellular identities in a genetic network. *Cell* **176**, 844-855 (2019).

23. S. Beyhan, F. H. Yildiz, Smooth to rugose phase variation in *Vibrio cholerae* can be mediated by a single nucleotide change that targets c-di-GMP signalling pathway. *Mol. Microbiol.* **63**, 995–1007 (2007).

24. D. Andrienko, Introduction to liquid crystals. *J. Mol. Liq.* **267**, 520–541 (2018).

25. C. Fei, S. Mao, J. Yan, R. Alert, H. A. Stone, B. L. Bassler, N. S. Wingreen, A. Košmrlj, Nonuniform growth and surface friction determine bacterial biofilm morphology on soft substrates. *Proc. Natl. Acad. Sci. USA* **117**, 7622–7632 (2020).

26. J. C. N. Fong, F. H. Yildiz, The *rbmBCDEF* gene cluster modulates development of rugose colony morphology and biofilm formation in *Vibrio cholerae*. *J. Bacteriol.* **189**, 2319–2330 (2007).

27. C. Absalon, K. Van Dellen, P. I. Watnick, A communal bacterial adhesin anchors biofilm and bystander cells to surfaces. *PLoS Pathog.* **7**, e1002210 (2011).

28. V. Berk, J. C. N. Fong, G. T. Dempsey, O. N. Develioglu, X. W. Zhuang, J. Liphardt, F. H. Yildiz, S. Chu, Molecular architecture and assembly principles of *Vibrio cholerae* biofilms. *Science* **337**, 236–239 (2012).

29. J. C. N. Fong, K. A. Syed, K. E. Klose, F. H. Yildiz, Role of *Vibrio* polysaccharide (vps) genes in VPS production, biofilm formation and *Vibrio cholerae* pathogenesis. *Microbiology* **156**, 2757–2769 (2010).

30. F. Beroz, J. Yan, Y. Meir, B. Sabass, H. A. Stone, B. L. Bassler, N. S. Wingreen, Verticalization of bacterial biofilms. *Nat. Phys.* **14**, 954–960 (2018).

31. F. M. Leslie, Some constitutive equations for liquid crystals. *Arch. Rational Mech. Anal.* **28**, 265–283 (1968).

32. B. Qin, C. Fei, A. A. Bridges, A. A. Mashruwala, H. A. Stone, N. S. Wingreen, B. L. Bassler, Cell position fates and collective fountain flow in bacterial biofilms revealed by light-sheet microscopy. *Science* **369**, 71–77 (2020).

33. M. A. A. Grant, B. Wacław, R. J. Allen, P. Cicuta, The role of mechanical forces in the planar-to-bulk transition in growing *Escherichia coli* microcolonies. *J. R. Soc. Interface* **11**, 20140400 (2014).

34. Z. You, D. J. G. Pearce, A. Sengupta, L. Giomi, Mono- to multilayer transition in growing bacterial colonies. *Phys. Rev. Lett.* **123**, 178001 (2019).

35. A. Doostmohammadi, J. Ignés-Mullol, J. M. Yeomans, F. Sagués, Active nematics. *Nat. Commun.* **9**, 3246 (2018).

36. Antony. N. Beris, B. J. Edwards, *Thermodynamics of flowing systems: with internal microstructure* (Oxford University Press, New York, 1994).

37. D. W. Thompson, *On Growth and Form* (Cambridge University Press, Cambridge, 1992).

38. K. Copenhagen, R. Alert, N. S. Wingreen, J. W. Shaevitz, Topological defects promote layer formation in *Myxococcus xanthus* colonies. *Nat. Phys.* **17**, 211–215 (2021).

39. T. B. Saw, A. Doostmohammadi, V. Nier, L. Kocgozlu, S. Thampi, Y. Toyama, P. Marcq, C. T. Lim, J. M. Yeomans, B. Ladoux, Topological defects in epithelia govern cell death and extrusion. *Nature* **544**, 212–216 (2017).

40. X. Jin, I. H. Riedel-Kruse, Biofilm lithography enables high-resolution cell patterning via optogenetic adhesin expression. *Proc. Natl. Acad. Sci. USA* **115**, 3698-3703 (2018).

**Acknowledgments:**

We thank Drs. A. Mashruwala and Y. Xu for their help in the initial experiments. We thank Drs S. Mao, T. Cohen, and J.-S. Tai for helpful discussions and B. Reed and M. Zhao for help with developing the ABSs.

**Funding:**

JY holds a Career Award at the Scientific Interface from the Burroughs Welcome Fund.

**Author contributions:**

JN and JY designed and performed the experiments. JN, QZ, HL, and JY analyzed data. CL and SZ developed the agent-based simulations. JN developed the continuum theory. JN, CL, SZ, and JY wrote the paper.

**Competing interests:**

The authors declare that they have no competing interests.

**Data and materials availability:**

Matlab codes for single-cell segmentation are available online at Github: https://github.com/Haoran-Lu/Segmentation_3D-processing/releases/tag/v1.0. Other data are available upon request.

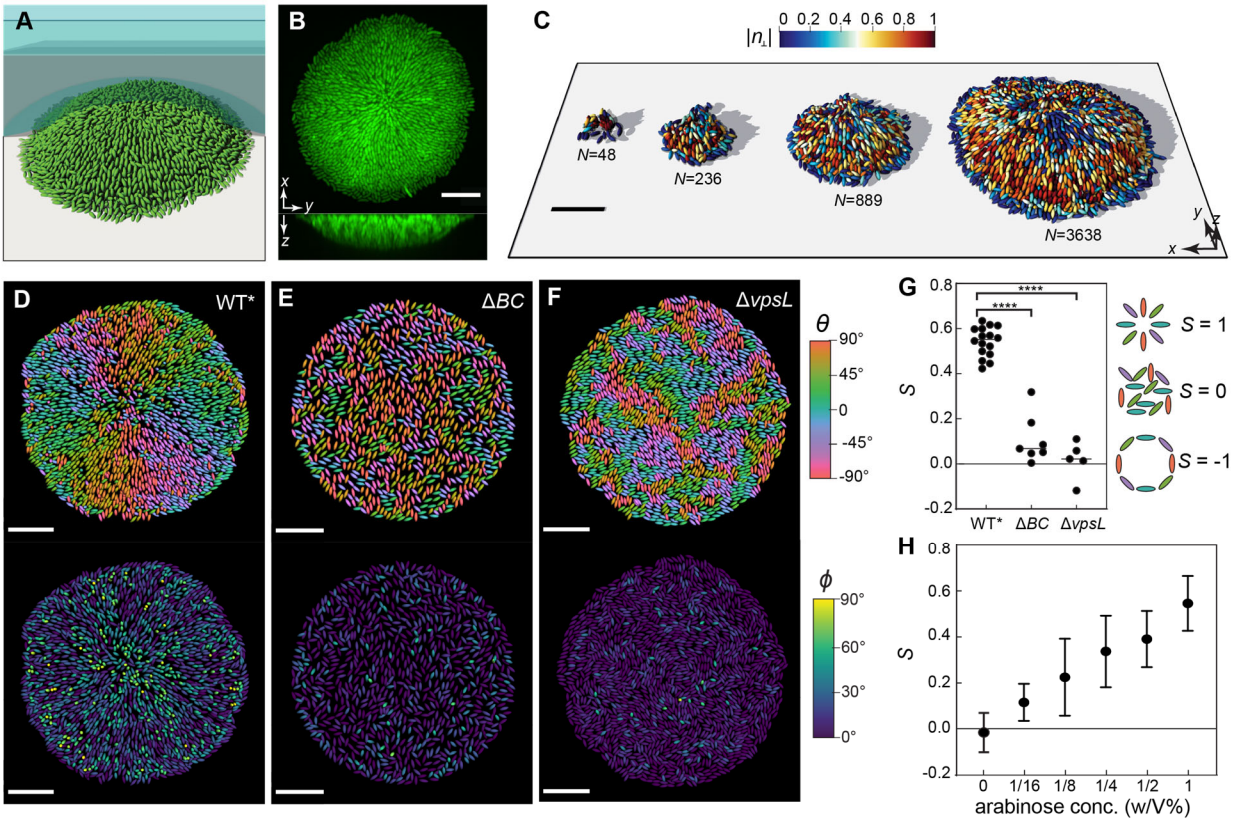


**Fig. 1: *V. cholerae* biofilms self-organize into aster patterns.** (**A**) Schematic of the experimental setup, where *V. cholerae* biofilms (green) were grown on a glass surface covered by a hydrogel (blue shaded). (**B**) Representative cross-sectional views of a WT* biofilm expressing mNeonGreen. (**C**) Single-cell 3D reconstruction of biofilm structures over time with different numbers of cells *N*. (**D** to **F**) Cell orientation color-coded according to each cell's angle in the basal plane $\theta$ (*Top*) or the angle it makes with the substrate $\phi$ (*Bottom*), (D) in a biofilm that produces both exopolysaccharides and surface adhesion proteins (WT*), (E) in a biofilm that only produces exopolysaccharides (Δ*BC*), and (F) in a bacterial colony with neither exopolysaccharides nor surface adhesion (Δ*vpsL*). Scale bars, 10 μm. (**G**) Radial order parameter *S* quantifying the degree to which cells conform to an aster pattern in the three strains. Data was subjected to ANOVA for comparison of means. ****denotes P<0.0001. (**H**) *S* in biofilms in which the expression of *rbmC* is controlled by an arabinose inducible promotor.

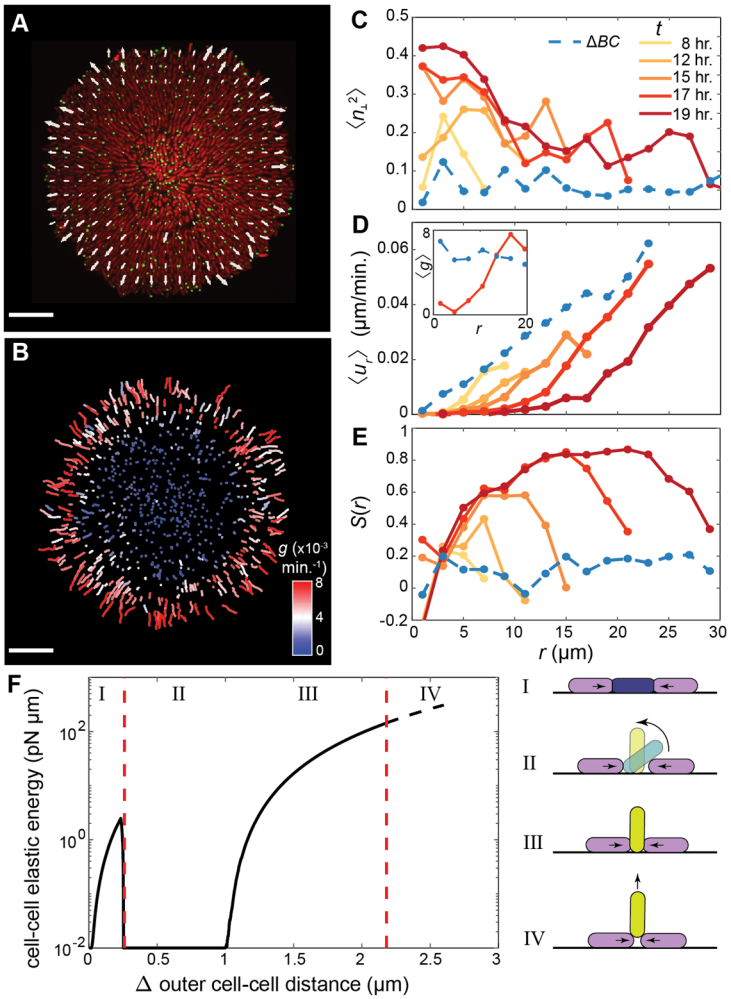


**Fig. 2: Growth-induced cellular flow and surface anchoring jointly lead to aster formation in biofilms.** (**A**) Raw image of the basal layer of a biofilm consisting of cells constitutively expressing mScarlet-I cytosolically and mNeonGreen-labelled puncta. Overlain is the velocity field measured from puncta trajectories. (**B**) Puncta trajectories colored by the apparent in-plane growth rate $g$. The apparent in-plane growth rate is calculated as $g(r) = (\partial_r r u_r)/r$ in a neighborhood around each cell. Scale bars, 10 μm. (**C** to **E**) Azimuthally averaged (C) degree of verticalization $\langle n_\perp^2 \rangle$, (D) radial velocity $\langle u_r \rangle$ (Inset: apparent in-plane growth rate $\langle g \rangle \times 10^{-3}\text{min.}^{-1}$), and (D) radial order parameter $S$ as a function of distance $r$ from the center, in the basal layer. The dashed blue lines denote results from the nonadherent mutant. (**F**) Results of a

reduced problem showing the strain energy due to cell-to-cell contacts in a cell as it is squeezed by two neighbors (black line). The dashed red lines denote the results from stability analyses (Supplementary Text). Upon increasing compression, the central cell evolves through four phases, which are given schematically.

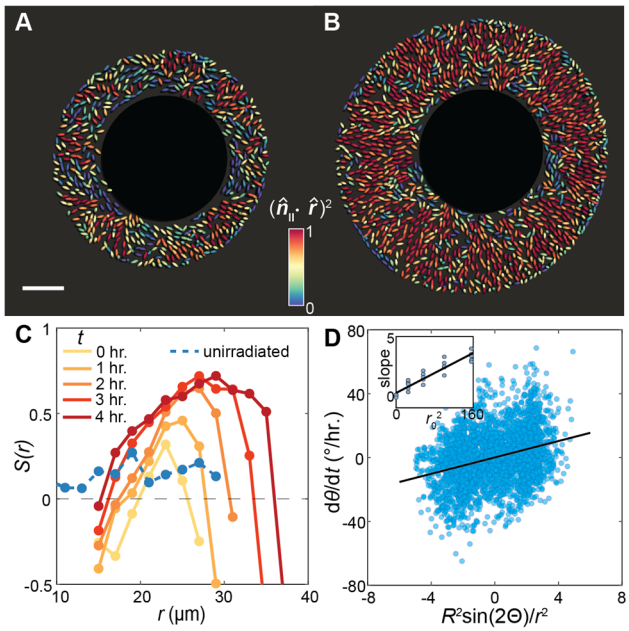


**Fig. 3: Cell organization can be manipulated by controlling spatial growth patterns.** (**A**, **B**) A nonadherent biofilm grown for 17 hours was irradiated using 405 nm laser to induce cell death in a circle of radius 15 μm at the center. Colors denote the degree of radial alignment of individual cells $(\hat{\boldsymbol{n}}_{\parallel}\cdot\hat{\boldsymbol{r}})^2$. (**C**) $S(r)$ in the irradiated biofilm (colored according to time) and the unirradiated control (blue). (**D**) Angular velocity of individual cells from ABSs with a growth void plotted against the predicted nondimensionalized driving force. Inset: Fitted slope from (D) for different growth void sizes $r_0$ (μm$^2$).

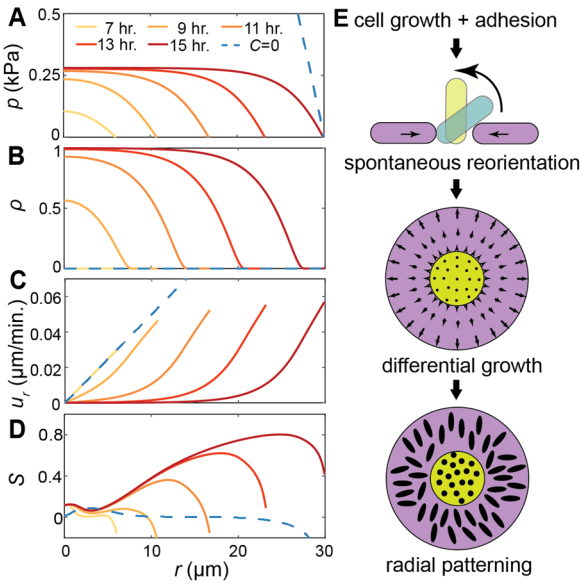


**Fig. 4: A two-phase active nematic model predicts spontaneous generation of differential proliferation and macroscopic cell organization.** (**A** to **D**) Numerical solution of the model consisting of a population of horizontal and vertical cells. The biofilm was initiated with no vertical cells and random in-plane orientations. Evolution of (A) pressure $p$, (B) fraction of vertical cells $\rho$, (C) in plane radial velocity $u_r$, and (D) radial order parameter $S$. Curves are colored according to time. Results for a biofilm that cannot sustain verticalized cells ($C = 0$) are shown in blue. (**E**) Schematic representation of the biofilm self-patterning process.